Solid phase recrystallization induced by multi-pulse nanosecond laser annealing

Pablo Acosta Alba, Joris Aubin, Sylvain Perrot, Fulvio Mazzamuto, Adeline Grenier, Sébastien Kerdilès

Applied Surface Science Advances 3 (2021) 100053

Contents lists available at ScienceDirect

Applied Surface Science Advances

journal homepage: www.elsevier.com/locate/apsadv

Solid phase recrystallization induced by multi-pulse nanosecond laser annealing

Pablo Acosta Alba[a,*], Joris Aubin[b], Sylvain Perrot[b], Fulvio Mazzamuto[b], Adeline Grenier[a], Sébastien Kerdilès[a]

[a] Université Grenoble Alpes, CEA-LETI, 38000 Grenoble, France
[b] SCREEN-LASSE, 92230 Genneviliers, France

A B S T R A C T

The solid phase recrystallization of partially amorphized SOI structures using a pulsed Ultra-Violet Nanosecond Laser Annealing (UV-NLA) is reported. It is shown that combining UV-NLA process with a heating chuck at low temperature (450 °C) results in the perfect recrystallization of the amorphized portion of the silicon layer. Actually, sub-melt multi-pulse UV-NLA enables obtaining the total crystal recovery and a very high dopant activation rate, comparable to melt laser annealing approaches or high temperature rapid thermal annealing, with a very low overall thermal budget. This approach is a great alternative to traditional solid phase epitaxial regrowth process, which reach it limits, in terms of recrystallization rate, at temperatures lower than 500 °C. The process presented here is thus suitable for integration paths in which the thermal budget must be limited as for example 3D sequential integration. Besides the high activation rate, another benefit of the solid phase recrystallization, compared to an equivalent laser anneal in the melt regime, is the almost unchanged surface roughness. Furthermore, the use of an in-situ metrology based on Time Resolved Reflectometry (TRR) enables the monitoring of the crystalline seed thickness evolution during UV-NLA and the estimation of the recrystallization rate.

1. Introduction

Epitaxial recrystallization of ion implanted semiconductors layers is a required process step in current integration paths. Actually, ion implantation is a remarkable technique for well controlled doping in semiconductors. However, the introduction of highly energetic ions into the crystal disturbs its lattice, causing damage and even amorphisation at sufficiently high implantation doses. In any case, post-implantation annealing step is required to recover crystallinity and enable dopant activation through the diffusion of dopant atoms onto substitutional lattice sites. Pulsed laser annealing was, for the first time, used to induce the epitaxial regrowth and replace the standard post-implantation annealing of amorphized samples around the mid-1970s [1,2].

Nowadays, the semiconductor industry must address a continuously increasing number of challenges related to device scaling such as, diffusion control, doping level and conformality, buried devices' layer integrity. In particular, the introduction of three-dimensional (3D) architectures combined with the use of new materials requires the reduction of the overall thermal budget in the whole integration flow. In a 3D sequential integration with at least two stacked levels of active devices, dopant activation in the upper level without degradation of the underlying devices is a real challenge since classical annealing techniques are not anymore compatible. In this context, Ultra-Violet Nanosecond Laser Annealing (UV-NLA) provides a promising alternative to more established methods as for example furnace or Rapid Thermal Annealing (RTA).

The UV wavelength leads to a short absorption depth in silicon, while the nanosecond pulse duration limits the heat diffusion towards embedded structures, with a confinement of the heat in the very first nanometers [3–5]. In the last years, UV-NLA has been successfully explored for shallow junction formation [6,7] or contact resistance reduction [8,9]. Most of these studies deal with the liquid phase recrystallization regime with side effects on surface roughness and transport of matter [10]. In contrast, solid phase recrystallization has been less explored. In general, scanning continuous wave lasers (e.g. Ar ion lasers) with dwell times in the millisecond range, cause local heating of the near surface region of Si to temperatures approaching the melting point. This laser annealing enables the thermally induced solid phase recrystallization of amorphous layers on a crystalline substrate [11,12]. Usually, this growth mechanism is explained by the extrapolation of the regrowth conditions of rapid thermal annealing, which is the most traditional and well-understood method for treating post-implantation damage in silicon [13]. Compared to traditional furnace annealing, the regrown crystalline layer after continuous wave laser irradiation was shown to exhibit several interesting and desirable properties. Most notably, it was demonstrated that, as a result of the localized heating and rapid heating/cooling rates, limited diffusion occurs [11] and the electrical dopant activation rate might reach almost 100% even when the dopant concentration exceeds the solid solubility limit [14]. This highlights the relevance to use the laser annealing approach. However, additional re-

* Corresponding author.
E-mail address: pablo.acostaalba@cea.fr (P. Acosta Alba).

https://doi.org/10.1016/j.apsadv.2020.100053
Received 30 September 2020; Received in revised form 17 December 2020; Accepted 23 December 2020
Available online 7 January 2021

Table 1
Ion implantation conditions leading to the formation of an amorphous layer in the near surface region.

Dopant	Energy [keV]	Dose [at/cm^2]	Expected a-Si thick. [nm]
As	9	1×10^{15}	14.0 ± 0.4
P	4	1×10^{15}	10.5 ± 0.4
B (PAI Ge)	6 (7)	1×10^{15} (5×10^{14})	12.2 ± 0.4

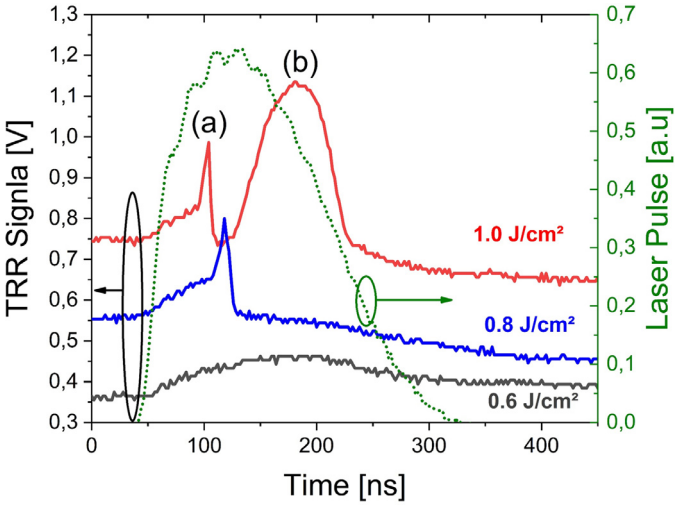

Fig. 1. Laser pulse (right axis) and time resolved reflectometry (TRR) profiles (left axis) recorded during UVNLA. Data for a phosphorous implanted SOI sample laser annealed at various energy densities. Labelled peaks correspond to (a) the melt and explosive recrystallization and (b) the 'second' melt.

searches are required in order to reduce further the thermal budget and reach a higher performance.

The aim of this work is to participate improving this method by using still lower thermal budgets thanks to nanosecond laser pulses. Hereafter, we demonstrate that low energy density multi-pulse UV-NLA can be used to induce the solid phase recrystallization of amorphized doped silicon layers in the sub-melt regime.

2. Experimental procedure

Blanket 300 mm Silicon-On-Insulator (SOI) substrates with 12 nm of Si on top (CZ, p-type, 10–20 ohm.cm) and 20 nm of buried oxide (Box) were used as starting material. The thickness of the silicon top layer was increased to 22 nm. First a 30 s HF(5%)/HCl wet cleaning was applied in order to get rid of native oxide. Then, Si epitaxy was performed in a reduced pressure CVD tool. Afterwards, the surface of three wafers was prepared by wet cleaning and then the wafers were implanted in a Viista HCP ion implanter with As, P or B ions (with Ge Pre-Amorphisation Implantation) at the fluence of 1×10^{15} at/cm^2 and respective energies of 9, 4 and 6 keV. These ion implantation conditions enabled the formation of a thin amorphous Si (a-Si) layer (<20 nm). Ion implantation conditions and amorphized thicknesses are summarized in Table 1. Afterwards, samples were submitted to UV-NLA in a SCREEN LT-3100 tool with a XeCl excimer laser (λ=308 nm) with a 160 ns pulse duration (full width at half maximum, see Fig. 1) and a repetition rate of 4 Hz. The laser beam is spatially homogenized (<3% uniformity) in order to obtain a 15×15 mm^2 top-hat beam. Using this laser annealing, different regions were irradiated with a single pulse and an increasing laser energy density ranging from 0.36 to 1.80 J/cm^2. The wafer temperature was maintained at 450 °C thanks to a heating chuck. Afterwards, in the second part of the study, multi-pulse laser treatments have been assessed. To do that, several shots at fixed energy density have been cumulated on a single position. It is worth noting that different locations

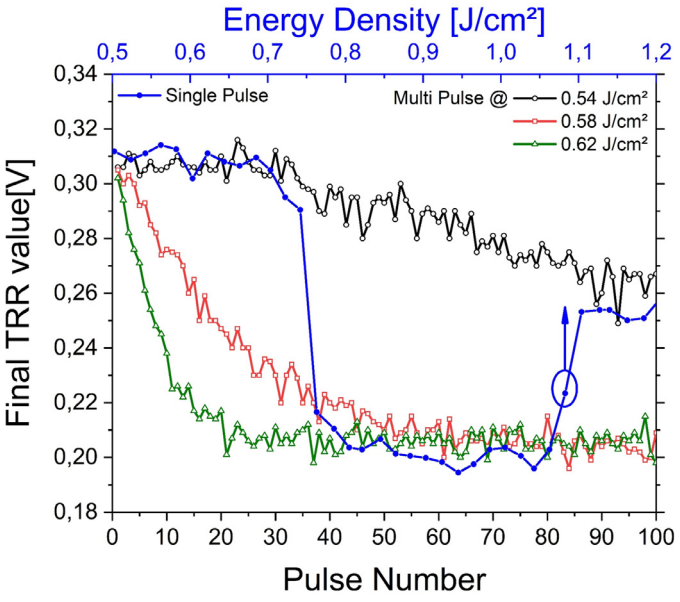

Fig. 2. Final TRR signal (solid ● top axis) as a function of the energy density using a single pulse irradiation, and final TRR value evolution as a function of the number of pulses for sub-melt laser conditions (open symbols, bottom axis). Phosphorous implanted SOI sample.

on the wafer have been used for this multi pulse study. Each location corresponding to a specific number of cumulated pulses.

In-situ Time Resolved Reflectometry (TRR) based on a 635 nm wavelength laser enabled us to collect the light reflected by the annealed surface during UVNLA. This in-situ metrology was used to detect the phase change of the near surface material, a-Si layer in our case. Indeed, the reflected light intensity dramatically increases when the silicon layer melts. TRR enables to clearly identify the laser energy density thresholds for which a transition occurs, such as the explosive melt of the amorphous layer [15] or the total melt of the SOI layer. Surface roughness was assessed through Atomic Force Microscopy, with 10×10 μm^2 and 1×1 μm^2 scans performed on a Dimension FastScan platform from Bruker. Samples were also submitted to sheet resistance measurements using a 4 point-probe NAPSON WS3000 tool.

3. Results and discussion

The laser pulse profile and measured TRR intensity during UVNLA are shown in Fig. 1. The TRR signal has been shifted by 0.2 V for each Energy Density (ED) to facilitate readability. For a low ED of 0.60 J/cm^2, there was almost no evolution of the TRR signal. The weak bump is most likely due to heating then cooling of the sample. The reflectivity increase upon heating is likely due to an evolution with the temperature of the optical and thermal properties of a-Si. For higher ED (≥ 0.80 J/cm^2), two characteristic features can be observed. The first peak, labeled (a) in Fig. 1, corresponds to the a-Si melt and explosive recrystallization phenomenon, with the formation of a poly-Si. This is a well-known phenomenon occurring due to the thermodynamic instability of molten a-Si which is associated to an under-cooled material [9]. This is especially relevant during the UV-NLA of amorphous semiconductor materials due to the exothermic amorphous-liquid-crystal transition. The second peak, labeled (b), is associated with the melt of the poly-Si obtained after explosive recrystallization named 'second melt' below [17]. The use of the TRR signal enables a clear identification of different transition thresholds.

The explosive melt threshold was found to be around 0.74 J/cm^2 for phosphorous implanted samples and 0.66 J/cm^2 for arsenic or boron (Ge PAI) implanted ones. Differences are likely due to amorphized thick-

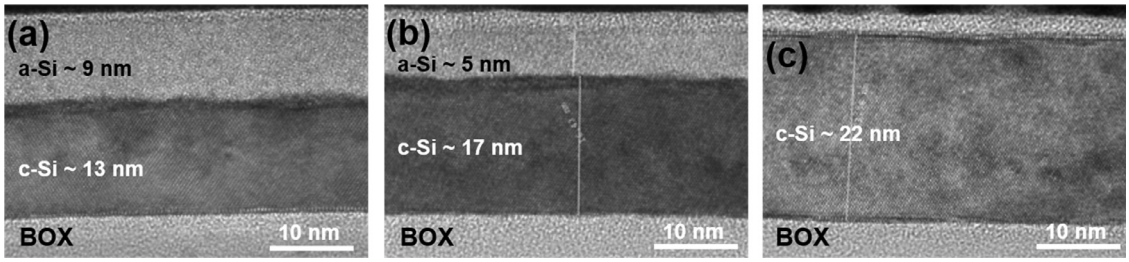

Fig. 3. Cross sectional TEM images of 22 nm thick SOI structures (a) as-Phosphorous -implanted and after sub-melt multi pulse UV-NLA at 0.58 J/cm^2 with (b) 30 or (c) 100 cumulative shots.

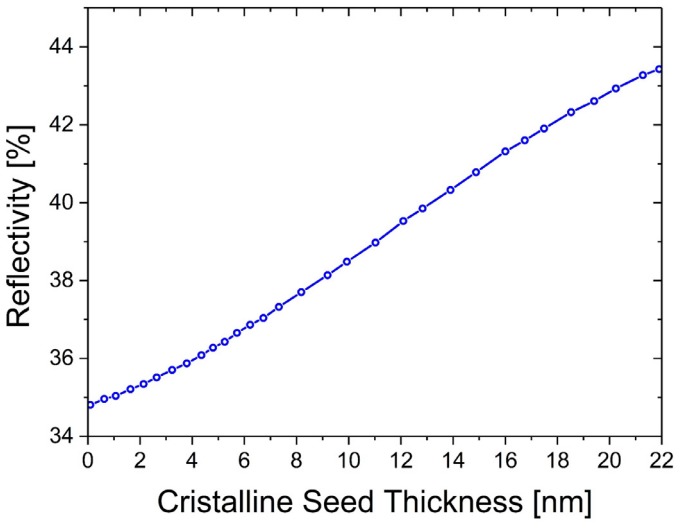

Fig. 4. Reflectivity evolution of the 22 nm thick Silicon-On-Insulator structure. The crystalline seed thickness varies from 0 to 22 nm. Meanwhile, the amorphous silicon layer on top has a thickness such that the sum of the two is always 22 nm, i.e. the starting thickness.

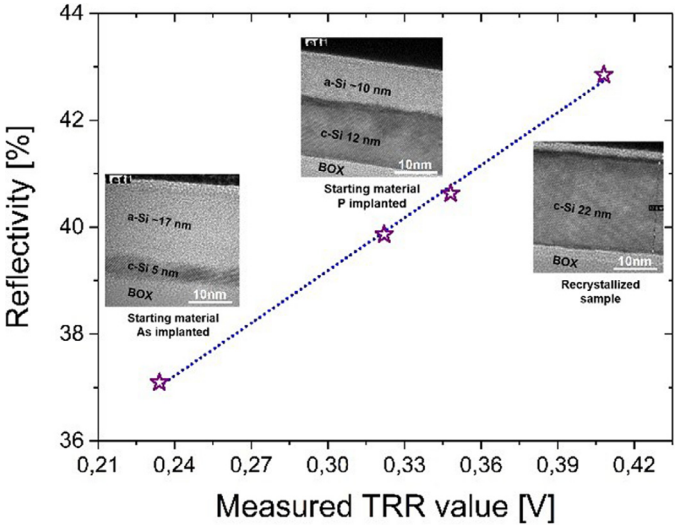

Fig. 5. Calculated reflectivity versus measured TRR signal value for known samples. The linear relationship between expected reflectivity and TRR signal enables to determine the crystalline seed thickness.

ness differences. Since only sub-melt conditions are to be used for solid phase epitaxial recrystallization, once the explosive melt and second melt thresholds were identified, wafers were always irradiated using sub-melt multi-pulse irradiation conditions.

At the end of the TRR record, typically for $t > 400$ ns, the signal is representative of the final state of the structure and surface. The evolution of the final TRR signal as a function of ED is plotted in Fig. 2. For a single laser pulse (Fig. 2, solid points and top axis), the final TRR value is, at low ED (i.e. lower than the explosive threshold), close to the initial one (0.30 V, Fig. 1 left axis). For ED slightly higher than the explosive melt threshold, the final TRR value drops down to 0.22 V. In the ED range between 0.76 J/cm^2 and 1.05 J/cm^2, the final TRR value drops down to 0.20 V. Finally, for ED higher than 1.05 J/cm^2, it increases once again to 0.25 V. These three different behaviors can be explained by the material structure after UV-NLA.

In a previous work [6], we showed that single pulse UV-NLA on similar samples yielded to different structures depending on the ED.

(i) For ED lower than the explosive threshold (0.76 J/cm^2), the irradiated structure did not change;
(ii) For ED between explosive threshold and full melt (1.05 J/cm^2 here), the liquid phase recrystallization from the crystalline seed led to a monocrystalline Si layer with a very low density of structural defects;
(iii) For ED higher than the full melt threshold, UV-NLA resulted in the melt of the entire crystalline seed, with the formation of a poly-Si layer.

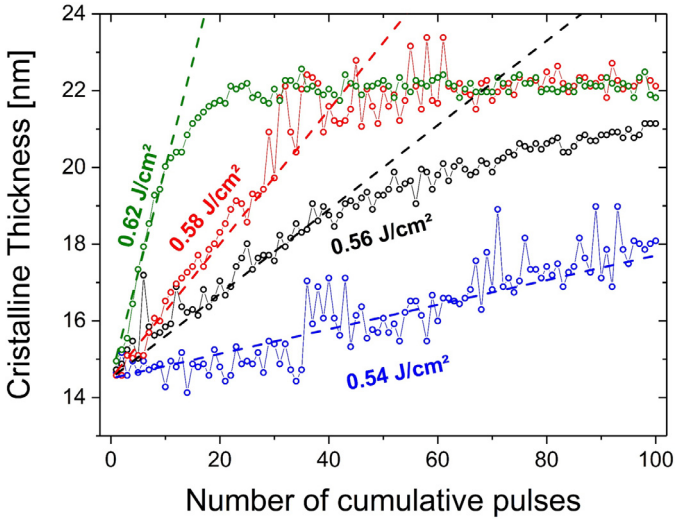

Fig. 6. Crystalline Si thickness versus number of pulses, for an As-implanted SOI sample, as extracted from the TRR evolution measured during laser annealing.

The TRR final value of 0.20 V thus corresponds to a fully recrystallized 22 nm thick SOI layer. Additionally, the a-Si layer remained amorphous after single pulse UVNLA at low ED, showing that single pulse UVNLA below the melt threshold was not able to induce solid phase recrystallization [6,16,17].

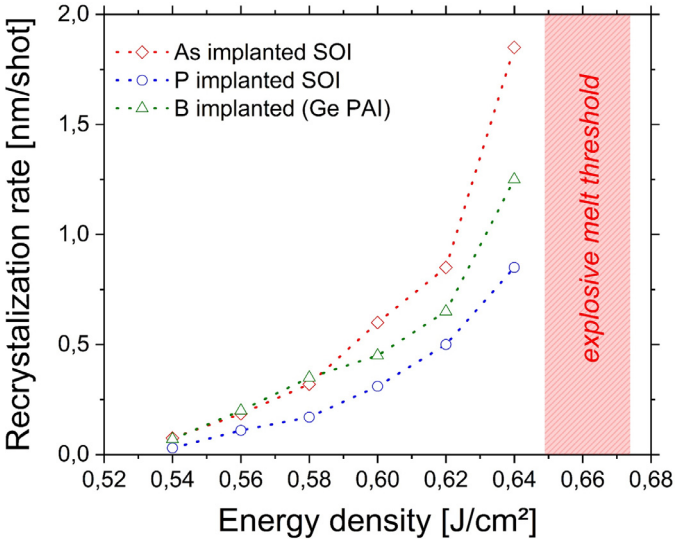

Fig. 7. Recrystallization rate for different energy densities and for all samples studied in this work.

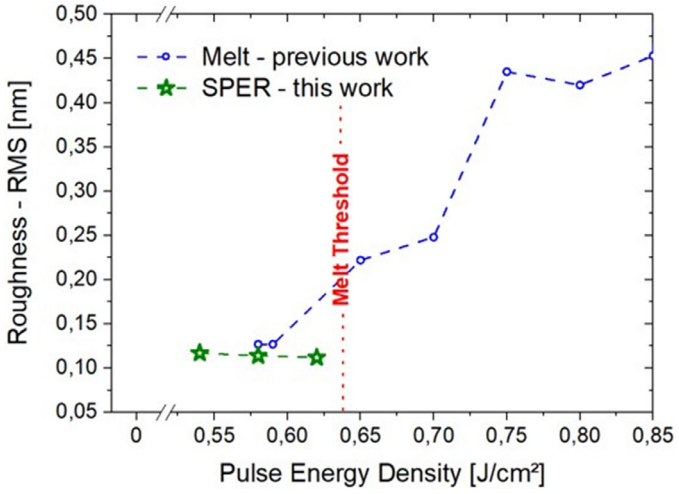

Fig. 8. Surface roughness RMS values from AFM scans (i) in the melt regime (from the single pulse approach) and (ii) after sub-melt solid phase recrystallization with multi pulse irradiation.

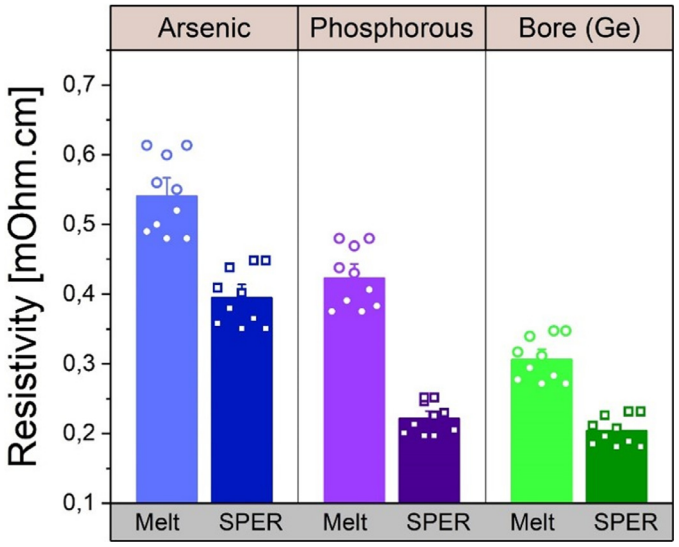

Fig. 9. Resistivity obtained from sheet resistance measurements for each dopant.

Hence, multi-pulse sub-melt UV-NLA was explored with EDs lower than the explosive threshold. Fig. 2 also shows the evolution of the final TRR value for multi-shots laser annealing (open symbols) as a function of the number of pulses for three energy densities. The TRR value gradually drops down to 0.20 V for ED = 0.62 J/cm^2 (~80% of the melt threshold) corresponding to the TRR level expected for a crystalline silicon top layer after recrystallization. For lower ED (0.58 J/cm^2), the evolution of the final TRR value is slower. It nevertheless reaches the TRR level corresponding to the complete recrystallization. For even lower ED (0.54 J/cm^2), this evolution is much slower, with a TRR intensity which can be associated which a partial recrystallization of the a-Si layer.

Fig. 3 shows cross-section Transmission Electron Microscopy (TEM) images of the phosphorous implanted sample. These observations confirm the scenario proposed from the TRR signal evolution. TEM shows that 30 cumulated laser pulses at 0.58 J/cm^2 results in a partial recrystallization of the amorphous Si layer. In contrast, when 100 pulses are cumulated at the same ED, the entire amorphous silicon layer is recrystallized. This clearly shows that the UV-NLA in a sub-melt multi-pulse mode with the assistance of a heating chuck at 450 °C can result in a progressive solid phase recrystallization of the amorphous layer from the crystalline seed.

Furthermore, the TRR recorded signal can be used in order to estimate the recrystallization rate. Based on the Fresnel equations, we can calculate the theoretical reflectivity of stacks corresponding to the studied samples consisting of a bulk silicon, a 20 nm thick silicon dioxide layer and a top silicon stack made of an amorphous and a crystalline layer, its total thickness always being 22 nm. The calculated reflectivity is shown in Fig. 4. Then, we can also plot the expected reflectivity as a function of the TRR signal value measured on various known samples. The linear relationship between the measured TRR intensity and the calculated reflectivity value is obvious in Fig. 5. We can then calculate the expected reflectivity for each TRR after each laser pulse. From this reflectivity value, we can then obtain the seed thickness expected for each sample. Fig. 6 shows the evolution of the expected crystalline seed thickness as a function of the number of cumulative laser shots for various ED. The slope of these curves provides the recrystallization rate (in nm per shot). There is a strong increase of the recrystallization rate when the ED increases.

Based on this methodology, the recrystallization rate evolution as a function of ED is plotted in Fig. 7 for samples implanted with As, P and B (and Ge PAI). It shows a rapid increase of the recrystallization rate with ED. A recrystallization rate of 1.5 nm/pulse can be obtained for ED still lower than the explosive melt threshold, which is extremely fast given the pulse duration (160 ns).

Two expected advantages of solid phase recrystallization approach should be a limited degradation of the surface roughness and a high dopant activation. Fig. 8 shows the Root Mean Square (RMS) value extracted from AFM measurements for both solid and liquid phase recrystallization approaches. For UV-NLA conditions leading to the a-Si layer recrystallization with both approaches (ED around 0.80 J/cm^2 for the melt conditions [6]), the surface roughness is lower with the solid phase recrystallization approach. Finally, we can also compare the resistivity obtained with both approaches. Resistivity was calculated from sheet resistance (Rs) measurements of the various samples. Since the resistivity value is extracted from sheet resistance measurements, we must use an accurate thickness value for each sample. For the melt approach, the lowest Rs is obtained in the 'near total melt' regime. It thus means that the melt depth is very close to the total thickness of the top silicon layer (22 nm), with an uniform distribution of dopants in the entire layer. In contrast, activated dopants are expected to be mostly in the recrystallized layer in the solid phase approach, since no dopant diffusion is expected during UV-NLA. The conducting layer thickness was thus as-

sumed to be close to the amorphization depth (after ion implantation) with this approach (see Table 1 for values). Fig. 9 shows the resistivity calculated from Rs measurements with such an assumption.

The resistivity with the solid phase recrystallization approach is then systematically lower than with the melt approach.

Multi-pulse UVNLA with sub-melt conditions thus yields very promising results in terms of recrystallization rate, surface roughness evolution and dopant activation levels, all this with a very low thermal budget compatible with 3D-sequential integration.

4. Conclusions

In this work, we demonstrated the solid phase recrystallization on partially amorphized SOI layers with an extremely low thermal budget. Indeed, UV nanosecond laser annealing, whose short absorption depth and nanosecond scale pulse duration, greatly limits the thermal budget and the heat diffusion towards embedded structures. For the first time, this annealing technique is used in a multi-pulse mode with low energy densities (lower than the melt threshold), to progressively recrystallize SOI layers partially amorphized by ion implantation. This leads to very high dopant activation rate, comparable to that obtained by high temperature RTA processes or liquid phase epitaxy. Since the recrystallization is obtained in the solid phase, the surface roughness remains at very low levels. Furthermore, the analysis of in-situ time resolved reflectometry (TRR) enables estimating the recrystallization rates (nm/pulse) for different dopants as a function of the laser energy densities. For all these reasons, the annealing approach presented in this work seems to be a very promising alternative to post implantation annealing in new integration flows in which the thermal budget reduction is mandatory, as for example 3D sequential integration.

Declaration of Competing Interest

The authors declare that they have no known competing financial interests or personal relationships that could have appeared to influence the work reported in this paper.

Acknowledgments

The authors would like to thank Dr. J-M. Hartmann and Mrs. Marianne Coig from CEA-LETI for silicon layers epitaxy and ion implantation respectively. The authors also would like to thank SCREEN company and its French subsidiary SCREEN-LASSE for helping in operating and maintaining the LT-3100 laser annealing platform.

References

[1] G.A. Kachurin, N.B. Pridachin, L.S. Smirnov, Annealing of radiation defects by laser radiation pulses, Sov. Phys. Semicond. 9 (7) (1975).
[2] J.W. Mayer, J.M. Poate, Laser Annealing of Semiconductors, Academic Press, New York, USA, 1982 L.
[3] L. Brunet, et al., Breakthroughs in 3D Sequential technology, in: Proceedings of the IEEE International Electron Devices Meeting (IEDM), San Francisco, CA, 2018, pp. 7.2.1–7.2.4, doi:10.1109/IEDM.2018.8614653.
[4] C. Fenouillet-Beranger, et al., A review of the full 500°C low temperature technological modules development for high performance and reliable 3D sequential integration, in: Proceedings of the Electron Devices Technology and Manufacturing Conference (EDTM), Singapore, Singapore, 2019, pp. 249–251, doi:10.1109/EDTM.2019.8731192.
[5] A. Vandooren, et al., 3D sequential low temperature top tier devices using dopant activation with excimer laser anneal and strained silicon as performance boosters, VLSI (2020) 978-1-7281-6460-1.
[6] P. Acosta Alba, et al., Nanosecond laser annealing for phosphorous activation in ultra-thin implanted silicon-on-insulator substrates, in: Proceedings of the 21st International Conference on Ion Implantation Technology (IIT), Tainan, 2016, pp. 1–4, doi:10.1109/IIT.2016.7882896.
[7] K. Huet, et al., Doping of semiconductor devices by laser thermal annealing, Mater. Sci. Semicond. Process. 62 (2017) 92–102, doi:10.1016/j.mssp.2016.11.008.
[8] H. Shin, M. Lee, E. Ko, H. Ryu, S. Park, E. Kim, D. Ko, Dopant activation of in situ phosphorus-doped silicon using multi-pulse nanosecond laser annealing, Phys. Status Solidi A 217 (2020) 1900988, doi:10.1002/pssa.201900988.
[9] J.J.P. Bruines, R.P.M. van Hal, H.M.J. Boots, A. Polman, F.W. Saris, Time-resolved reflectivity measurements during explosive crystallization of amorphous silicon, Appl. Phys. Lett. 49 (1986) 1160–1162, doi:10.1063/1.97453.
[10] C. Acosta-Zepeda, P. Saavedra, J. Bonse, E. Haro-Poniatowski, Modeling of silicon surface topographies induced by single nanosecond laser pulse induced melt-flows, J. Appl. Phys. 125 (2019) 175101, doi:10.1063/1.5053918.
[11] A. Gat, F. Gibbons, T. Magee, J. Peng, V.R. Deline, P. Williams, C.A. Evans Jr., Physical and electrical properties of laser-annealed ion-implanted silicon, Appl. Phys. Lett. 32 (5) (1978) 276–278.
[12] J.S. Williams, W.L. Brown, H.J. Leamy, J.M. Poate, J.W. Rodgers, D. Rousseau, G.A. Rozgonyi, J.A. Shelnutt, T.T. Sheng, Solid-phase epitaxy of implanted silicon by cw Ar ion laser irradiation, Appl. Phys. Lett. 33 (6) (1978) 542–554.
[13] W.O. Adekoya, M. Hage-Ali, J.C. Muller, P. Siffert, On the kinetics of solid phase regrowth and dopant activation during rapid thermal annealing of implantation amorphized silicon, J. Appl. Phys. 64 (2) (1998) 666–676.
[14] A. Lietoila, J.F. Gibbons, T.W. Sigmon, The solid solubility and thermal behavior of metastable concentrations of As in Si, Appl. Phys. Lett. 36 (9) (1980) 765–768.
[15] S.F. Lombardo, S. Boninelli, F. Cristiano, I. Deretzis, M.G. Grimaldi, K. Huet, E. Napolitani, A. La Magna, Phase field model of the nanoscale evolution during the explosive crystallization phenomenon, J. Appl. Phys. 123 (2018) 105105, doi:10.1063/1.5008362.
[16] W. Yang, J. Mathews, J.S. Williams, Hyperdoping of Si by ion implantation and pulsed laser melting, Mater. Sci. Semicond. Process. 62 (2017) 103–114.
[17] F.C. Voogt, R. Ishihara, F.D. Tichelaar, Melting and crystallization behavior of low-pressure chemical-vapor-deposition amorphous Si films during excimer-laser annealing, J. Appl. Phys. 95 (2004) 2873–2879, doi:10.1063/1.1642286.